materials

MDPI

Article

Characterization of an Amorphous Titanium Oxide Film Deposited onto a Nano-Textured Fluorination Surface

Pei-Yu Li [1], Hua-Wen Liu [1], Tai-Hong Chen [2], Chun-Hao Chang [2], Yi-Shan Lu [1] and Day-Shan Liu [1,*]

[1] Institute of Electro-Optical and Materials Science, National Formosa University, Huwei, Yunlin 63201, Taiwan; 10476106@gm.nfu.edu.tw (P.-Y.L.); Neroliu0416@gmail.com (H.-W.L.); dream13130766@yahoo.com.tw (Y.-S.L.)

[2] ITRI South, Industrial Technology Research Institute, Liujia Shiang, Tainan 73445, Taiwan; a0922639175@gmail.com (T.-H.C.); tsaicc1221@gmail.com (C.-H.C.)

* Correspondence: dsliu@sunws.nfu.edu.tw; Tel.: +886-5-6315665

Academic Editor: Shoou-Jinn Chang
Received: 6 May 2016; Accepted: 26 May 2016; Published: 31 May 2016

Abstract: The photocatalytic activity of an amorphous titanium oxide (a-TiO_x) film was modified using a two-step deposition. The fluorinated base layer with a nano-textured surface prepared by a selective fluorination etching process acted as growth seeds in the subsequent a-TiO_x deposition. A nanorod-like microstructure was achievable from the resulting a-TiO_x film due to the self-assembled deposition. Compared to the a-TiO_x film directly deposited onto the untreated base layer, the rate constant of this fluorinate-free a-TiO_x film surface for decomposing methylene blue (MB) solution that was employed to assess the film's photocatalytic activity was markedly increased from 0.0076 min^{-1} to 0.0267 min^{-1} as a mechanism for the marked increase in the specific surface area.

Keywords: photocatalytic activity; two-step deposition; amorphous titanium oxide; nano-textured surface

1. Introduction

Titanium oxide (TiO_x) is one of the most popular materials in environmental purification, anti- or high-reflection coating, dye-sensitized solar cells, surface self-cleaning/antifogging functional coating, and biomedical engineering applications due to its chemical stability, optical transparency at visible wavelength, high refractive index, non-toxic nature, and low cost [1–5]. In terms of the photocatalytic activity, TiO_x film is known to be influenced by its crystalline structure, specific surface area, and functional group incorporation [6,7]. Although the TiO_x film with anatase structures has the best photocatalytic activity, the deposition and/or post-annealing temperature required to form anatase crystallinity is too high to limit such film applied to surface modification and packaging on the heat-sensitive substrates or devices. Accordingly, an effort was made to enhance the photocatalytic activity of an anatase-TiO_x film at low temperature by realizing the *p-n* junction or doping with a specific dopant [8–10]. Alternatively, an amorphous TiO_x film abundant in hydroxyl (O–H) functional groups on the film surface was found to be a promising substitute for exhibiting quality photocatalytic activity at a low temperature [11,12]. In our previous report, we developed a selectively fluorinated etching on the a-TiO_x film to result in a nano-textured surface with the incorporation of fluorine ions [13]. Such film exhibited a high photocatalytic activity that was comparable to that of the TiO_x film with an anatase structure and was applied to package the blue-light organic light emitting diode to result in a device with a self-cleaning function [14]. The apparent improvement on the film's photocatalytic activity was a mechanism of the formation of the Ti–F functional group for facilitating

the separation of the photo-produced charge couples and the increase in the reactants' adsorption as a consequence of the large specific surface area. However, since the fluorine ion is not environment friendly for the most chemically reactive and electronegative of all the elements, it becomes increasingly necessary to prepare a fluorine-free surface of the a-TiO_x film with the same photocatalytic activity by further optimizing the film's specific surface area. Accordingly, the above-mentioned process should be improved to realize a quality a-TiO_x film without the incorporation of the fluorine ions.

As the surface property of the a-TiO_x film was modifiable by the selectively fluorinated etching, in this work, a base layer with such a nano-textured surface abundant in fluorine ions affecting the subsequently deposited a-TiO_x film was studied. The growth mechanism of the resulting a-TiO_x film with the fluorine-free surface prepared using this two-step deposition was elucidated through the observations of the associated surface and cross-section morphologies. The origin responsible for the improvement of the photocatalytic activity was characterized by an increase in the specific surface area and amounts of OH groups as conducted from the measurements of the surface roughness and chemical bond configuration.

2. Experimental Procedure

A 100-nm-thick hydro-generated a-TiO_x film was deposited on silicon substrates (10×10 mm^2) by a plasma-enhanced chemical vapor deposition (PECVD) system, using a titanium tetraisopropoxide [$Ti(OC_3H_7)_4$, TTIP]-oxygen gas mixture. The deposition pressure, power, and gas flow rate of TTIP/O_2 were controlled at 40 Pa, 100 W, and 120/20 sccm, respectively. A detailed system setup and deposition parameters have been described elsewhere [12]. Incorporating fluorine ions into the nano-textured surface on the a-TiO_x film was achieved by pre-irradiating a UV light for 5 h through an anodic alumina membrane mask and then etching in the diluted hydrofluoric (HF) solution for a different time. The selective fluorination etching (hereafter abbreviated to SFE) has been addressed elsewhere [13]. A 100-nm-thick a-TiO_x film using PECVD under the same deposition condition was then coated onto the base layer with surface nano-textures to realize the a-TiO_x film surface free of the fluorine ions. In addition, another set of the a-TiO_x film crystallized into anatase structures was prepared by post-annealing the un-treated a-TiO_x film at 500 °C for 30 min under oxygen ambient (hereafter denoted as annealed TiO_x film) as a comparison.

Film thickness of these a-TiO_x films with and without the SFE treatment as well as prepared using the two-step deposition was measured using a surface profile system (Dektak 6M, Veeco, New York, NY, USA). Surface roughness was measured using atomic force microscopy (AFM, DI-3100, Veeco, New York, NY, USA) with the tapping mode. The surface and cross-section morphologies were observed by a field emission scanning electron microscope (FE-SEM, JSM-6700F, JEOL, Tokyo, Japan) operated at 3 kV. Fourier transform infrared spectrometry (FTIR, FT/IR-4100, JASCO, Halifax, NS, Canada) and X-ray photoelectron spectroscope (XPS, ULVAC-PHI, Quantera SXM, Kanagawa, Japan) with monochromatic Al $K\alpha$ radiation were employed to examine the film's chemical bonding states and surface bond nature. The photocatalytic activity for the a-TiO_x and annealed TiO_x films illuminated by the UV light with a constant intensity of 1 mW/cm^2 was evaluated by the decolorization of a 20 ppm concentrated methylene blue (MB) solution using the UV-Vis spectrophotometer from the absorbance of the resulting solution at 665 nm under atmosphere ambient.

3. Results and Discussion

Figure 1 shows the etching thickness of the a-TiO_x film with and without the UV light pre-irradiation for 5 h, and then immersed in the HF etching solution for different etching times. The etching thickness of the a-TiO_x film treated by additive UV light pre-irradiation was apparently lower than the a-TiO_x film directly etched by the HF solution. The less acidic surface of the a-TiO_x film, as a consequence of the Ti(IV)−OH, transformed into a Ti(III)−OH^- group due to the generated electrons under UV light pre-irradiation, was responsible for the alleviation of the sequential etching process [13]. A large discrepancy occurred in the etching thickness between the a-TiO_x films with and

without the UV light pre-irradiation (approximately 46 nm) as the etching time reached 35 s, while at this time the 100-nm-thick a-TiO_x film directly etched by the HF solution was almost completely removed, as shown in Figure 1. Because an apparent difference in the etching thickness of the a-TiO_x films was obtainable from the fluorination etching with and without UV light pre-irradiation, a selective fluorination etching treatment on the a-TiO_x film to modify its surface morphology was carried out by selectively shadowing the surface through a nano-sized mask with UV light pre-irradiation and then processing the fluorination etching.

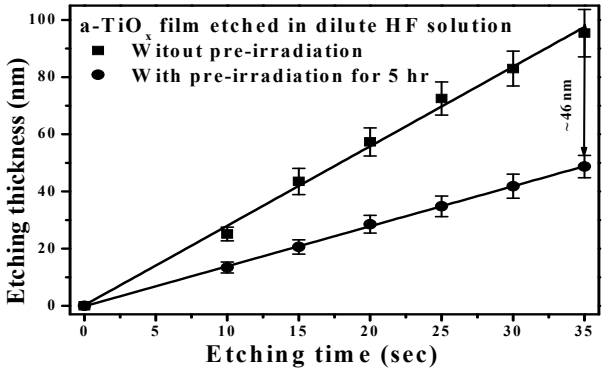

Figure 1. Etching thickness of the a-TiO_x film with and without the UV light pre-irradiation and then immersed in the HF etching solution for different etching times.

Figure 2b–d show the surface roughness of the a-TiO_x film selectively etched by the HF solution for 10, 20, and 35 s, respectively (the un-treated a-TiO_x film is given in Figure 2a for comparison). The untreated a-TiO_x film exhibited a smooth surface with a roughness of about 1.84 nm, whereas an increase in the surface roughness was obtained from the a-TiO_x films treated by the additive SFE process. The voids on the a-TiO_x surface gradually became visible as the SFE-treated time increased. Notable pinnacles and valleys were then clearly observed from the surface of the a-TiO_x film treated by the SFE process for 35 s, which corresponded to a very high surface roughness of 22.47 nm.

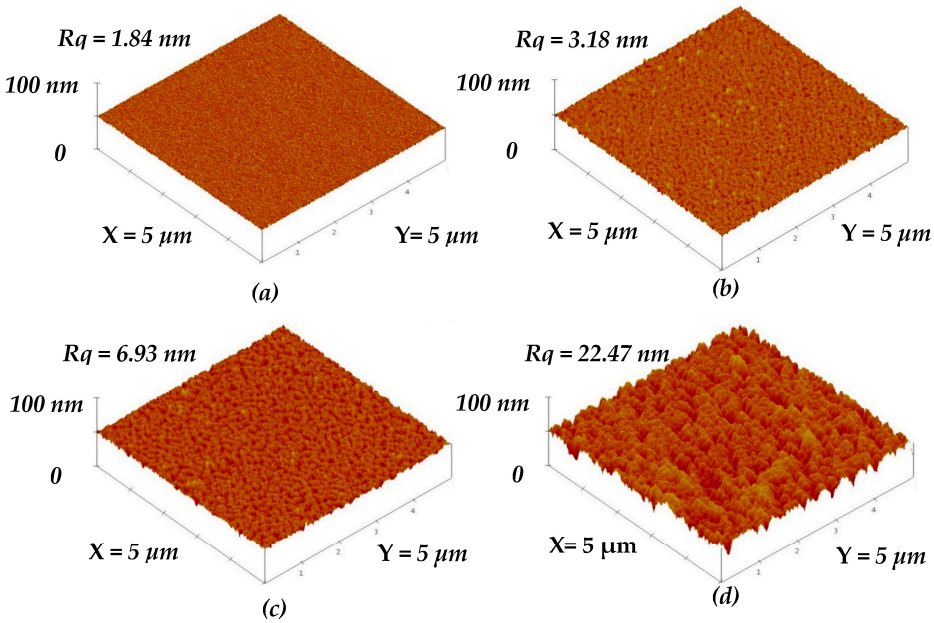

Figure 2. Surface roughness of the (**a**) un-treated a-TiO_x film; and SFE-treated a-TiO_x film for (**b**) 10; (**c**) 20; and (**d**) 35 s; respectively.

The surface morphologies of the untreated a-TiO_x film and the films treated by the SFE process for 10, 20, and 35 s, respectively, are shown in Figure 3a–d. As shown in Figure 3a, the particles on the untreated a-TiO_x surface are distributed densely and abnormally, whereas these particles observed from the a-TiO_x film surface processed by the SFE treatment for 10 s became separated with a round-like shape. The SFE process also resulted in these particles being uniformly distributed with an average diameter of about 20 nm, which was similar to the porous size of the AAM mask, as shown in the inset figure. Fine particles were then observed from the a-TiO_x film surface as it was further treated by the SFE process for 20 s (Figure 3b). The sidewall etching that led to the overcut profile was one possible reason why these particles appeared on the surface, evolving from a round-like to a needle-like shape. Meanwhile, the corresponding surface roughness of the a-TiO_x film also increased from 3.18 to 6.93 nm, as measured from Figure 2c. When the SFE treatment on the a-TiO_x film reached 35 s, the surface morphology also showed definite boundaries in addition to the fine particles. Referring to the etching thickness of the a-TiO_x film given in Figure 1, the obvious and wide boundaries were attributed to the regions of the a-TiO_x film that was completely removed from the substrate after etching by the HF solution without additive UV light irradiation.

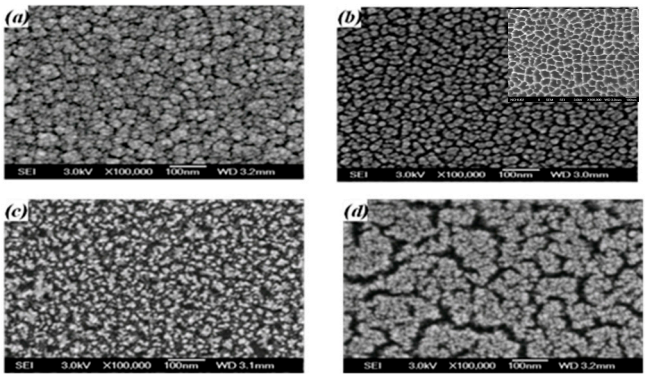

Figure 3. Surface morphologies of the (**a**) untreated a-TiO_x film; and SFE-treated a-TiO_x film for (**b**) 10; (**c**) 20; and (**d**) 35 s, respectively (the AAM patterns is provided in inset figure of Figure 3b).

These experiments demonstrated that the particles' shape and distribution on the a-TiO_x film surface were modifiable and controllable using the SFE treatment for different times. These base layers with surface nano-textures affecting the subsequent deposited a-TiO_x film were then investigated. Figure 4b–d give the surface roughness of the a-TiO_x films deposited onto the SFE-treated surface with nano-textures shown in Figure 2b–d, respectively, as well as the film deposited onto the untreated surface (Figure 4a). All the a-TiO_x films prepared using this two-step deposition process exhibited a higher surface roughness than that of their base layers shown in Figure 2a–d. The surface roughness of the a-TiO_x film deposited onto the untreated surface increased slightly to 2.27 nm. In contrast, a marked increase in the surface roughness was measured from the a-TiO_x film deposited onto the SFE-treated surface. The rougher the surface of the base layer obtained, the higher the increase in the roughness of the subsequently deposited a-TiO_x film. In addition, features of the pinnacles and valleys appearing on the surface of the a-TiO_x film deposited onto the surface treated with SFE for 35 s (Figure 4d) became more visible compared to those observed from the surface of its base layer (Figure 2d).

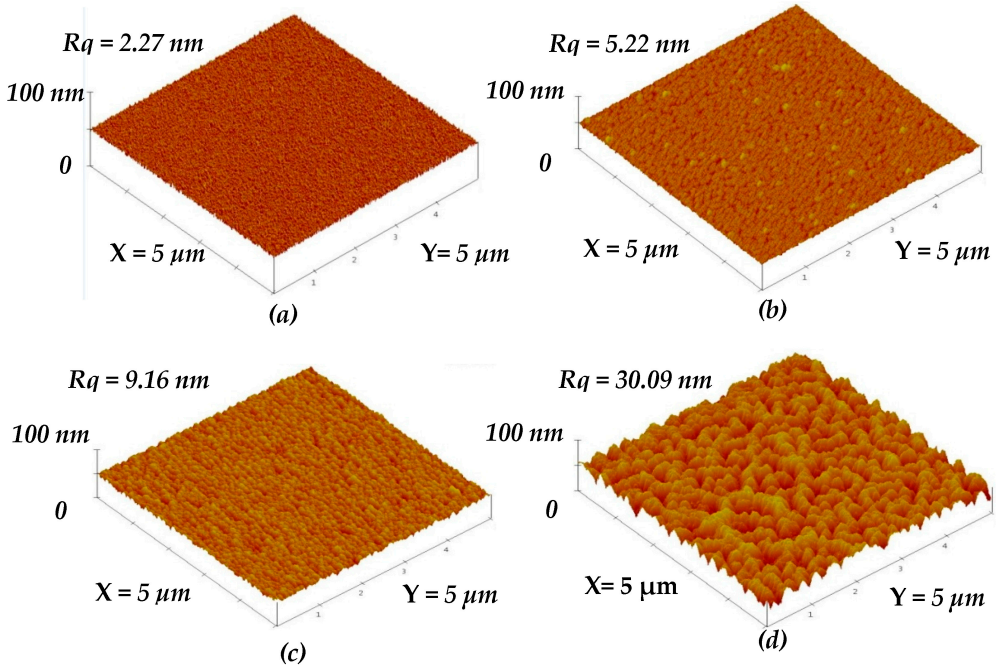

Figure 4. Surface roughness of the a-TiO_x film deposited onto (**a**) untreated base layer; and SFE-treated base layers for (**b**) 10; (**c**) 20; and (**d**) 35 s; respectively.

The corresponding surface morphologies shown in Figure 4 conducted from SEM measurements are presented in Figure 5a–d. The surface morphology of the a-TiO_x film deposited onto the untreated surface (Figure 5a) was almost identical to the film deposited onto the substrate on which the particles were distributed randomly and densely as presented in Figure 3a. For the a-TiO_x film deposited onto the surface with round-like particles, as shown in Figure 3b, the particles appearing on the a-TiO_x film (Figure 5b) had an average diameter apparently larger than those distributed over the base layer's surface, although their shape and distribution were quite similar. This suggested that the nuclei of the subsequently deposited a-TiO_x film were prone to forming and growing along the particles distributed over the base layer. The growth of particles on the a-TiO_x film became closer and resulted in the considerable increase in the surface roughness. For the a-TiO_x film deposited onto the surface shown in Figure 3c, the nuclei growing along the needle-like structure resulted in the particles on the a-TiO_x film surface evolving into a round-like shape with visible boundaries. As the surface morphologies of the two-step a-TiO_x films were deeply relevant to the particles on the base layer, the distributions of the significant channels and clusters observed from the a-TiO_x film shown in Figure 5d consisted of the growth of the fine particles and the enhancement of the boundaries appearing on the base layer shown in Figure 3d.

The cross-section micrographs shown in Figure 6a,b give further insights into the growth of the a-TiO_x film prepared using the two-step deposition process. In Figure 6a, random and dense fiber-like structures can be seen in both a-TiO_x layers, which had a definite interface, as indicated by arrows. This implied that the untreated base layer would not cause a structural change in the subsequently deposited a-TiO_x film. In contrast, the cross-section of the two-step a-TiO_x film shown in Figure 6b exhibited the feature of nanorod-like structures with no significant interface, confirming that the growth mechanism of the a-TiO_x film deposited onto the SFE-treated base layer was completely different from the film deposited onto the untreated base layer. The dimension of these nanorod-like structures was found to be widened with the growth of the two-step a-TiO_x film. Combined with their surface morphologies (Figures 3d and 5d), the particles on the base layer achieved using the SFE treatment were likely to act as growth seeds for the subsequent a-TiO_x deposition, thereby resulting in the upper a-TiO_x film, demonstrating conformity in the base layer with the increase in the surface roughness.

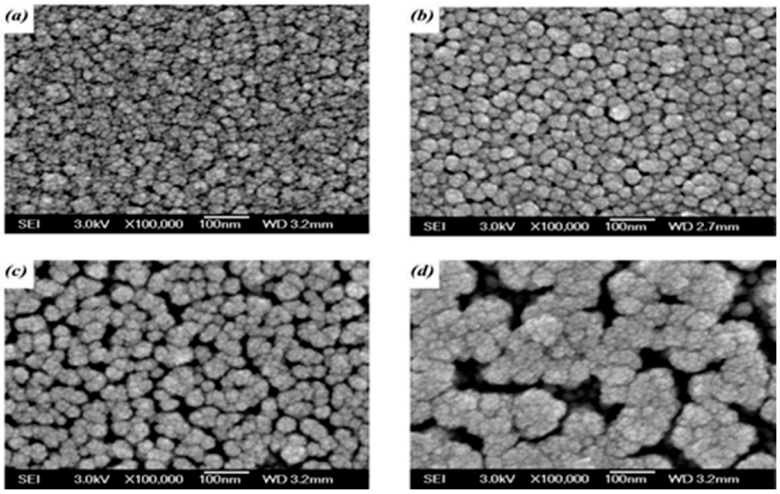

Figure 5. Surface morphologies of the a-TiO_x film deposited onto (**a**) untreated base layer; and SFE-treated base layers for (**b**) 10; (**c**) 20; and (**d**) 35 s; respectively.

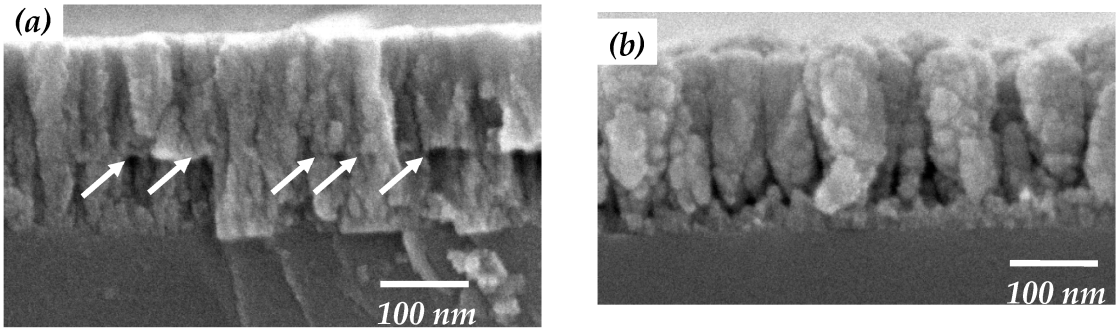

Figure 6. Cross-section images of the a-TiO_x film deposited onto (**a**) untreated; and (**b**) SFE-treated base layers (the arrows in Figure 6a mark the interface of the two-step deposited a-TiO_x film).

FTIR spectra of the base layer with and without an additive SFE treatment and the a-TiO_x films prepared using two-step deposition are illustrated in Figure 7a–d, respectively (Figure 7e) also shows the FTIR spectrum of the annealed TiO_x film for comparison). Both the untreated and SFE-treated base layers, as shown in Figure 7a,b, respectively, consisted of the fingerprint peak of the Ti–O bond around 400–800 cm^{-1} with the functional group of hydroxyl (OH) around high wavenumbers (2800–3700 cm^{-1}) [12]. The SFE treatment also caused the base layer to emit an additive signal at about 820 cm^{-1}, which was associated with the Ti–F vibration mode [13]. In addition, the incorporation of the fluorine ions into the base layer led to a shift of the O-H bond from 3450 to 3275 cm^{-1} due to an increase in the surface acidity. When the a-TiO_x film was deposited onto the SFE-treated base layer, the Ti–F bond was hardly observed in the FTIR spectrum (Figure 7d). Compared with the FTIR spectrum of the a-TiO_x film deposited onto the untreated base layer (curve c), both spectra only featured Ti–O and O–H bonds with almost the same peak position, except for a higher relative O-H bond intensity obtained from the a-TiO_x film deposited onto the SFE-treated base layer. Since the porous structures distributed in the low-temperature deposited oxidation film were the main reason responsible for the formation of the O–H groups [15,16], the reinforcement in the O–H bond obtained from the two-step deposition of the a-TiO_x coated onto the SFE-treated base layer thus implied the increase in the amounts of the pores. In addition, a sharp and intense Ti–O bond with the disappearance of the O–H bond as a consequence of the anatase crystallization was obtained from the FTIR spectrum of the annealed TiO_x film.

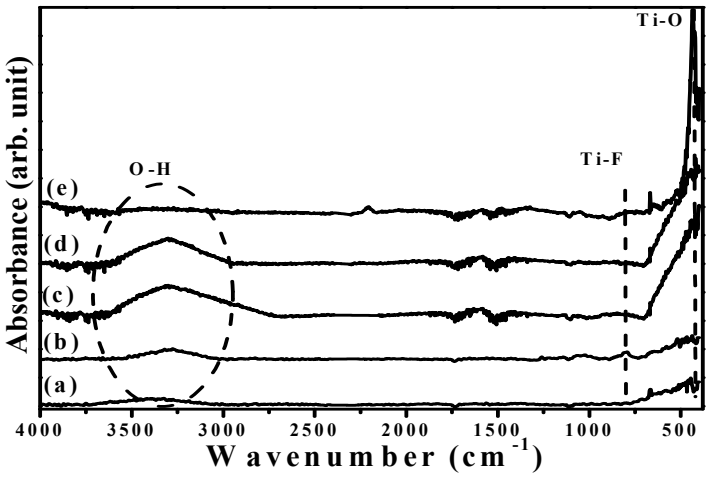

Figure 7. FTIR spectra of the (**a**) untreated; and (**b**) SFE-treated base layers and the a-TiO_x films deposited onto the (**c**) untreated; and (**d**) SFE-treated base layers; as well as (**e**) the annealed TiO_x film.

The binding energies related to the F 1*s*, Ti 2*p*, and O 1*s* core levels measured from the surface of the two-step deposited a-TiO_x film as well as the base layer are respectively illustrated in Figure 8a–c. Although a significant fluorine signal on the surface of the base layer emerged at about 684.9 eV, which was assigned to the Ti–F chemical bond due to the SFE treatment [17], this signal was absent in the surface of the subsequently deposited a-TiO_x film, indicating the achievement of the fluorine-free surface. In the Ti 2*p* spectrum (Figure 8b), both the peaks of the binding energies for the Ti $2p_{1/2}$ and Ti $2p_{3/2}$ occurred at approximately 464.6 and 458.9 eV, respectively, with a binding energy difference of 5.7 eV. A broad signal with a distinct satellite peak was observed from the binding energy of Ti $2p_{3/2}$ for the a-TiO_x film deposited onto the SFE-treated base layer, while this peak became sharp with a tail extending to the low binding energy in the spectrum of the a-TiO_x film deposited onto the untreated base layer. The peak of Ti $2p_{3/2}$ could be deconvoluted into two species of Ti^{4+} and Ti^{3+} ion states at 457.6 and 459.0 eV, respectively [18]. The composition of the Ti^{3+} to Ti^{4+} state (in the area of $Ti^{3+}/(Ti^{4+} + Ti^{3+})$), which was associated with the deficiency in the oxygen atoms on the surface, apparently increased from 0.29 to 0.39 as the a-TiO_x film was deposited onto the SFE-treated base layer. Regarding the O 1*s* spectra (Figure 8c), both surfaces of these two samples displayed an intense peak with a long tail extending to a high binding energy that could be deconvoluted into two feature peaks. The binding energy peak located at 530.6 eV was related to the Ti–O chemical bond, where the peak at the high binding energy of 531.8 eV emerged from the hydroxyl group (O–H) [19,20]. As determined from previous papers [21,22], the presence of the O-H bond indicated the termination of the chemical bond and/or contaminants and, thus, was responsible for the structural voids and boundaries. Accordingly, marked boundaries and voids observed from the surface and cross-section morphologies of the a-TiO_x film deposited onto the SFE-treated base layer were hydroxylated more intensely in the binding energy of O 1*s* (approximately 0.31, in the area of O–H/(Ti–O + O–H)) than those of the film deposited onto the untreated base layer (approximately 0.24).

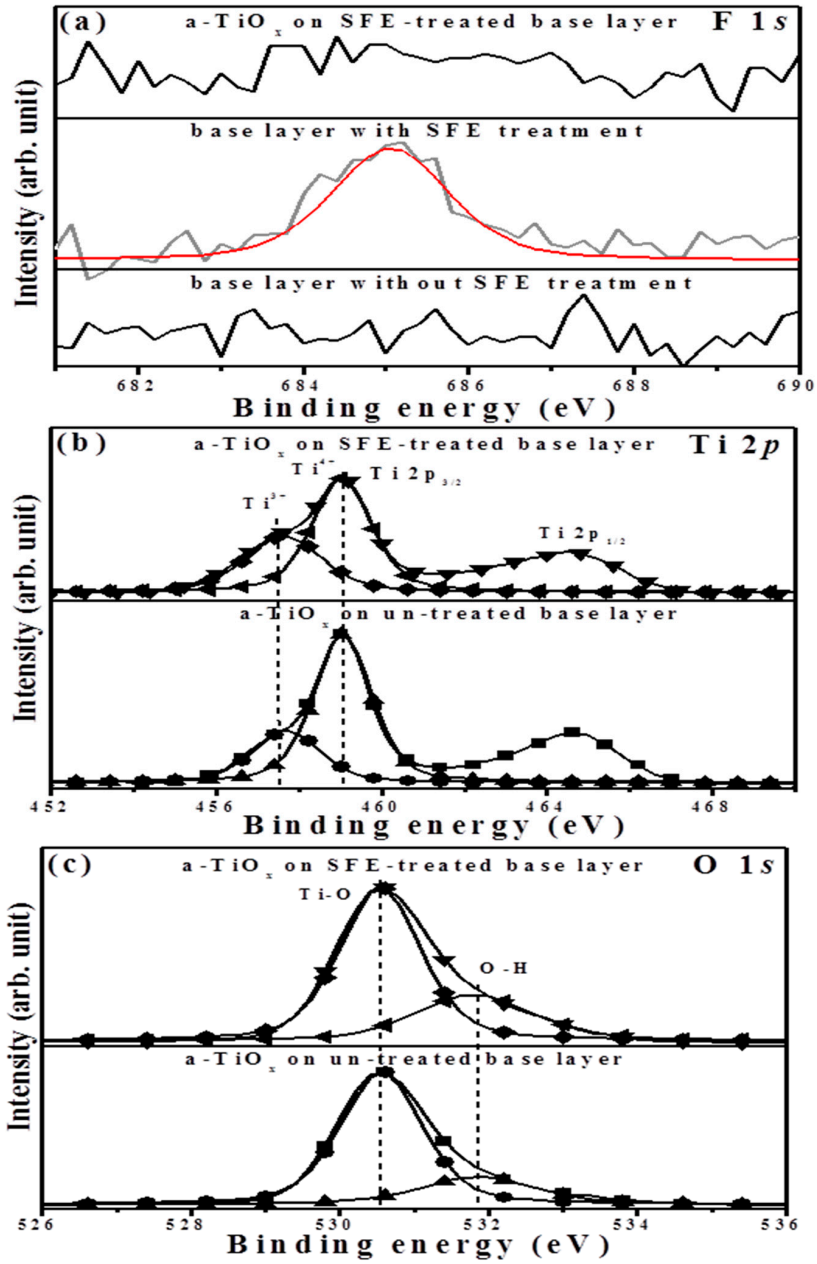

Figure 8. Binding energies related to the (**a**) F 1*s* core of the untreated and SFE-treated base layers as well as that of the a-TiO_x deposited onto the SFE-treated based layer; (**b**) Ti 2*p*; and (**c**) O 1*s* core levels of the a-TiO_x film deposited onto the untreated and SFE-treated base layers.

In addition, because the hydroxyl groups are beneficial for trapping hole carriers to suppress the recombination of the photo-generated electron-hole pairs, as demonstrated in previous studies [23,24], the a-TiO_x film deposited onto the SFE-treated base layer to degrade the MB solution, as depicted in Figure 9, is greatly improved compared to the same film deposited onto the untreated base layer. It is also worth noting that the a-TiO_x film with a surface free of the fluorine ions achieved using the two-step deposition even exhibited better efficiency in decomposing the MB solution than the annealed TiO_x film with anatase structures. The rate constant, k, which represents the quality of the photocatalytic activity of the film can be evaluated by fitting the curves shown in Figure 9, using the following relationship [25]:

$$\ln (C/C_0) = kt \quad (1)$$

where C and C_0 are the concentrations of the MB solution at a UV light irradiation time of $t = 0$ and t, respectively. The k value evaluated from each curve is denoted in Figure 9. Clearly, the a-TiO_x film deposited onto the SFE-treated base layer corresponded to a rate constant of 0.0267 min^{-1}, which was three times higher than the film deposited onto the untreated base layer (0.0076 min^{-1}) as well as a little higher than that of the annealed TiO_x film (0.0234 min^{-1}). According to the investigations into the morphologies and the analysis of the chemical bond configurations of the two-step deposited a-TiO_x film, the apparent roughening and nano-textured surface of the upper a-TiO_x film without the incorporation of the fluorine ions that grew by conforming along the particle seeds on the base layer surface, which was achieved using an additive SFE treatment, was the mechanism responsible for the great enhancement in the resulting photocatalytic activity.

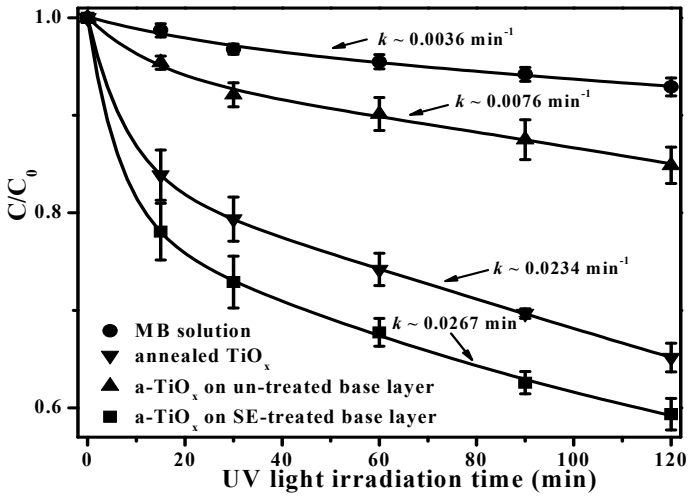

Figure 9. Photo-degradation to MB solution using a-TiO_x films deposited onto untreated and SFE-treated base layers as well as using the annealed TiO_x film (MB solution decomposed by the UV light irradiation also is shown for comparison).

4. Conclusions

The depth-dependent morphology of the surface-fluorinated a-TiO_x film was realized using an additive SFE treatment for different times. At the initial stage, the size and shape of these particles distributed over the a-TiO_x film surface after treatment with the SFE process for 10 s conformed to the patterns of the shadow mask. As the SFE treatment increased to 20 s, the shape of the particles appearing on the a-TiO_x film surface evolved from a round-like to a needle-like shape as a consequence of the apparent sidewall etching effect. Eventually, significant channels that corresponded to the film being completely removed from the substrate were observed from the a-TiO_x film processed by an additive SFE treatment for 35 s. The fluorinated surface with specific nano-textures of the a-TiO_x film acted as seed layer for the subsequently deposited a-TiO_x film according to the investigations of the surface and cross-section morphologies of the resulting a-TiO_x film. The nuclei of the a-TiO_x film self-assembled on the particles distributed over the SFE-treated base layer and then grew up to cause an apparent increase in surface roughness. Such roughening of the surface without the fluorine ion incorporation was achieved using the two-step deposition due to the deposition being selective, which also resulted in the film surface being abundant in the hydroxyl groups that were helpful for suppressing the recombination of the photo-generated electron-hole pairs. Accordingly, the fluorine-free a-TiO_x film deposited onto the SFE-treated base layer which had a nanorod-like structure possessing efficient photocatalytic activity, with a rate constant of 0.0267 min^{-1}; this was much higher than that of the film deposited on the untreated base layer (~0.0076 min^{-1}), as evaluated from these films photo-degrading in the MB solution.

Acknowledgments: This work was supported by the National Science Council and Industrial Technology Research Institute (ITRI South) under No. A200-105BA2 and the Ministry of Science and Technology under 105-2622-E-150-004-CC2.

Author Contributions: Day-Shan Liu organized and designed the experiment procedures; Tai-Hong Chen and Chun-Hao Chang wrote the paper; Pei-Yu Li and Hua-Wen Liu executed the film deposition; Yi-Shan Lu performed the thin film measurements and analysis. All authors read and approved the final version of the manuscript to be submitted.

Conflicts of Interest: The authors declare no conflict of interest.

References

1. Khan, S.U.M.; Al-Shahry, M.; Ingler, W.B., Jr. Efficient photochemical water splitting by a chemically modified n-TiO_2. *Science* **2002**, *297*, 2243–2245. [CrossRef] [PubMed]
2. Liu, D.S.; Lin, T.W.; Huang, B.W.; Juang, F.S.; Lei, P.H.; Hu, C.Z. Light-extraction enhancement in GaN-based light-emitting diodes using grade-refractive-index amorphous titanium oxide films with porous structures. *Appl. Phys. Let.* **2009**, *94*, 143502. [CrossRef]
3. Necula, B.S.; Fratila-Apachitei, L.E.; Zaat, S.A.J.; Apachitei, L.; Duszczyk, J. *In vitro* antibacterial activity of porous TiO_2–Ag composite layers against methicillin-resistant *Staphylococcus aureus*. *Acta Biomater.* **2009**, *5*, 3573–3580. [CrossRef] [PubMed]
4. Fang, Y.; Wang, X.; Ai, X.; Huang, J.; Wang, Q.; Wu, T. Sputtered TiO_x thin film as compact layer for solid-state dye sensitized solar cells. *Ceram. Int.* **2014**, *40*, 15941–15949. [CrossRef]
5. Kmetykó, Á.; Mogyorós, K.; Gerse, V.; Kónya, Z.; Pusztai, P.; Dombi, A.; Hernádi, K. Photocatalytic H_2 production using Pt-TiO_2 in the presence of oxalic acid: Influence of the noble metal size and the carrier gas flow rat. *Materials* **2014**, *7*, 7022–7038. [CrossRef]
6. Eufinger, K.; Poelman, D.; Poelman, H.; De Gryse, R.; Marin, G.B. Photocatalytic activity of dc magnetron sputter deposited amorphous TiO_2 thin films. *Appl. Surf. Sci.* **2007**, *254*, 148–152. [CrossRef]
7. Tian, G.; Fu, H.; Jing, L.; Tian, C. Synthesis and photocatalytic activity of stable nanocrystalline TiO_2 with high crystallinity and large surface area. *J. Hazard. Mater.* **2009**, *161*, 1122–1130. [CrossRef] [PubMed]
8. Su, Y.; Chen, S.; Quan, X.; Zhao, H.; Zhang, Y. A silicon-doped TiO_2 nanotube arrays electrode with enhanced photoelectrocatalytic activity. *Appl. Surf. Sci.* **2008**, *255*, 2167–2172. [CrossRef]
9. Wu, C.Y.; Hong, S.C.; Hwang, F.T.; Lai, L.W.; Lin, T.W.; Liu, D.S. Effect of nickel oxide seed layers on the annealed-amorphous titanium oxide thin films prepared using plasma-enhanced chemical vapor deposition. *Thin Solid Films* **2011**, *520*, 320–327. [CrossRef]
10. Chen, J.Z.; Chen, T.H.; Lai, L.W.; Li, P.Y.; Liu, H.W.; Hong, Y.Y.; Liu, D.S. Preparation and characterization of the surface photocatalytic activity with NiO/TiO_2 nanocomposite structure. *Materials* **2015**, *8*, 4273–4286. [CrossRef]
11. Hatanaka, Y.; Naito, H.; Kando, M. Photocatalytic characteristics of hydro-oxygenated amorphous titanium oxide films prepared using remote plasma enhanced chemical vapor deposition. *Appl. Surf. Sci.* **2005**, *244*, 554–557. [CrossRef]
12. Wu, C.Y.; Chiang, B.S.; Chang, S.; Liu, D.S. Determination of photocatalytic activity in amorphous and crystalline titanium oxide films prepared using plasma-enhanced chemical vapor deposition. *Appl. Surf. Sci.* **2011**, *257*, 1893–1897. [CrossRef]
13. Shih, P.C.; Huang, C.H.; Chen, T.H.; Lai, L.W.; Lu, Y.S.; Liu, D.S. Enhancement on Photocatalytic Activity of an Amorphous Titanium Oxide Film with Nano-Textured Surface by Selective-Fluorination Etching Process. *Mater. Res. Bull.* **2014**, *52*, 177–182. [CrossRef]
14. Chen, J.Z.; Chen, T.H.; Lai, L.W.; Huang, C.H.; Hong, S.C.; Liu, D.S. A quality photocatalytic activity of an amorphous titanium oxide film achieved using the selectively photochemical etching and its application for the organic light emitting diode encapsulation. *Microelectron. Eng.* **2015**, *148*, 5–9. [CrossRef]
15. Teshima, K.; Sugimura, H.; Inoue, Y.; Takai, O. Gas Barrier Performance of Surface-Modified Silica Films with Grafted Organosilane Molecules. *Langmuir* **2003**, *19*, 8331–8334. [CrossRef]
16. Yang, L.L.; Lai, Y.S.; Chen, J.S.; Tsai, P.H.; Chen, C.L.; Jason Chang, C. Compositional tailored sol-gel SiO_2–TiO_2 thin films: Crystallization, chemical bonding configuration, and optical properties. *J. Mater. Res.* **2005**, *20*, 3141–3149. [CrossRef]

17. Yu, J.; Wang, W.; Cheng, B.; Su, B.L. Enhancement of photocatalytic activity of mesporous TiO_2 powders by hydrothermal surface fluorination treatment. *J. Phys. Chem. C* **2009**, *113*, 6743–6750. [CrossRef]
18. Lin, X.; Rong, F.; Fu, D.; Yuan, C. Enhanced photocatalytic activity of fluorine doped TiO_2 by loaded with Ag for degradation of organic pollutants. *Powder Technol.* **2012**, *219*, 173–178. [CrossRef]
19. Domaradzki, J.; Kaczmarek, D.; Prociow, E.L.; Borkowska, A.; Schmeisser, D.; Beuckert, G. Microstructure and optical properties of TiO_2 thin films prepared by low pressure hot target reactive magnetron sputtering. *Thin Solid Films* **2006**, *513*, 269–274. [CrossRef]
20. Chen, S.; Zhang, S.; Wei, L.; Wei, Z. Preparation and activity evaluation of *p-n* junction photocatalyst NiO/TiO_2. *J. Hazard. Mater.* **2008**, *155*, 320–326.
21. Schuisky, M.; Kukli, K.; Aarik, J.; Lu, J.; Hårsta, A. Epitaxial growth of TiO_2 films in a hydroxyl-free atomic layer deposition. *J. Crystal Growth* **2002**, *235*, 293–299. [CrossRef]
22. Kumar, N.; Kozakov, A.T.; Dash, S.; Tyagi, A.K.; Lin, I.N. Microstructure, chemical bonds, and friction properties of nanocrystalline diamond films deposited in two different plasma media. *Phys. Solid State* **2013**, *55*, 2076–2087. [CrossRef]
23. Nakamura, M.; Kobayashi, M.; Kuzuya, N.; Komatsu, T.; Mochizuka, T. Hydrophilic property of SiO_2/TiO_2 double layer films. *Thin Solid Films* **2006**, *502*, 121–124. [CrossRef]
24. Xin, B.; Wang, P.; Ding, D.; Liu, J.; Ren, Z.; Fu, H. Effect of surface species on Cu-TiO_2 photocatalytic activity. *Appl. Surf. Sci.* **2008**, *254*, 2569–2574. [CrossRef]
25. Li, H.; Zhao, G.; Han, G.; Song, B. Hydrophilicity and photocatalysis of $Ti_1-xV_xO_2$ films prepared by sol–gel method. *Surf. Coat. Technol.* **2007**, *201*, 7615–7618. [CrossRef]